This paper appears in IEEE Transactions on Haptics 2014
DOI: 10.1109/TOH.2014.2346501

Design and Control of a Dual Unidirectional Brake Hybrid Actuation System for Haptic Devices

Carlos Rossa[1], José Lozada, and Alain Micaelli

***Abstract*— Hybrid actuators combining brakes and motors have emerged as an efficient solution to achieve high performance in haptic devices. In this paper an actuation approach using two unidirectional brakes and a DC motor is proposed. The brakes are coupled to overrunning clutches and can apply a torque in only one rotational direction. The associated control laws, that are independent of the virtual environment model, calculate the control gains in real time in order limit the energy and the stiffness delivered by the motor to ensure stability. The reference torque is respected using the combination of the motor and the brake. Finally, an user experiment has been performed to evaluate the influence of passive and active torque differences in the perception of elasticity. The proposed actuator has a torque range of 0.03 Nm to 5.5 Nm with a 17.75 kNm^{-2} torque density.**

1. Introduction

Haptics refers to the modality of touch and complementary sensory feedback. Researchers working in the area deal with the development of devices that allow human operators to sense and manipulate computer-generated or tele-operated environments through mechanical actuators. A haptic device must convey kinaesthetic stimuli from the environment to the operator with maximum transparency. Ideally, the operator must not be able to distinguish between the real world, e.g. holding a real object, and the virtual world, in which the same object is simulated [1].

Stability and transparency are key design requirements in haptics, stability is essential to the correct simulation of the environment and transparency is defined as the ratio of the desired and simulated impedance, where the ideal ratio is unity for a given bandwidth [2]. Therefore, the ideal display has no inertia and no friction, infinite bandwidth and is able to vary from zero to infinite output impedance while maintaining stability.

Haptic displays can be classified as either active or passive depending on the nature of the actuators used to generate the haptic stimuli.

Active interfaces commonly employ electric motors. Such actuators can restore and dissipate energy with a fast response time and relatively good control performance. However, the interaction with discrete environments requires the quantization of time, and the position or forces. Several authors have considered these issues for stable haptic interaction using active actuators. They have highlighted a critical tradeoff between the sampling rate, the simulated stiffness and energy dissipation due to viscous friction [3]. For instance, a stability condition for the simulation of a virtual wall modelled as a stiffness K and a damping B needs to satisfy the following inequality [4]:

$$b > \frac{KT}{2} + B \tag{1}$$

where b and T are the physical viscous friction coefficient and the sampling rate respectively. This equation implies that some physical energy dissipation is necessary to achieve stability, and it must be greater than the energy injected by the sampling delay. As a consequence, any active devices will exhibit a limited range of displayable impedance.

Due to their relatively low torque per volume ratio, motors are frequently linked to reduction stages. This dramatically increases the inertia and friction reflected at the end-effector. Though, inertial and frictional forces have to be reduced under the smallest human-detectable force threshold so that perception of the environment is not disturbed by the device [5]. Such dynamic effects can be compensated with admittance control schemes where force transducers and some minimal detectable inertia are required [6]. Admittance control provides good accuracy in free-motion but it can result in instability during the interaction with stiff environments [7]. A second solution consists of redesigning the mechanical device by replacing reduction stages with passive actuators.

Passive actuators, on the other hand, are intrinsically stable and safe. Passivity eliminates the risk of damaging or injuring the operator and this faculty is especially suitable for interactions involving high forces and velocities. Moreover, as most real or virtual environments can be modelled as passive, the haptic device is frequently used to dissipate the energy provided by the operator. In addition, passive actuators such as powder brakes, rheological brakes and dampers possess considerably higher torque densities and require less power compared to electric motors.

It can be concluded that the implementation of either active or passive actuators in haptic devices has antagonistic goals. Passive actuators are able to simulate passive elements with stability and safety but cannot restore energy. Conversely, active actuators can ensure energy restitution but can encounter several instability issues when conveying passive elements. Hybrid interfaces comprising both passive and active actuators are thereby a natural extension of haptic devices.

In the reported works dealing with hybrid actuators a brake and a motor are commonly linked in parallel. This arrangement is an efficient way to combine the torque capability of each actuator. However, the brake can block the motor and the system can behave as passive [8]. In contrast, in this paper an

The authors are with the French Atomic Energy Commission - CEA, LIST, Sensorial and Ambient Interfaces Laboratory, 91191 Gif-sur-Yvette, France.

[1]Corresponding author current address: Department of Electrical & Computer Engineering, University of Alberta, Edmonton T6G2V4, Canada. Email: rossa@ualberta.ca.

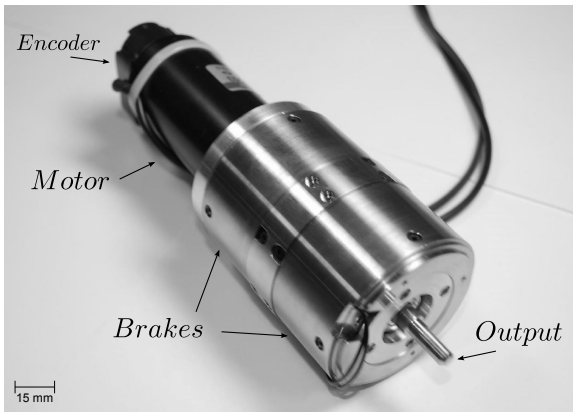

Fig. 1. Hybrid actuator composed of two identical unidirectional magnetorheological brakes and a commercial motor. The actuator has a torque range of 0.03 Nm to 5.5 Nm with 17.75 kNm^{-2} torque density.

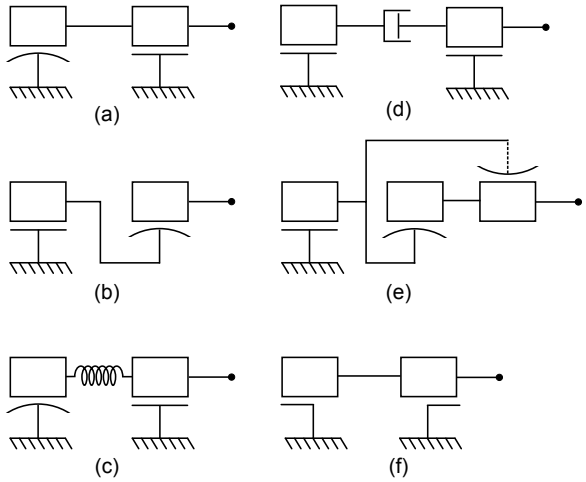

Fig. 2. Hybrid brake/motor configurations. A rectangle represents an inertia, two parallel lines represent a motor and a concave line represents a brake. A coil and a piston represents a spring and a damping respectively. A circle symbolises the end-effector. A half concave line indicates an unidirectional brake. A mechanical connection indicates that the velocity is the same on each side. Dashed lines indicate velocity inversion. Fig. adapted from [5].

actuation system based on unidirectional brakes is introduced. The paper is separated into three main parts. The first part focusses on the mechanical design. The actuator is composed of two custom-made brakes and a DC motor (see Fig. 1). Each brake is linked to an overrunning clutch so that a brake can apply a torque only in one direction. The second part addresses the associated control laws. An adaptive controller determines the control loop gains for each actuator in real time. It bounds the stiffness sent to the motor and use the brake to respect a reference torque. Finally, the paper presents a perceptual evaluation of passive and active torque asymmetry on the perception of stiffness.

2. Documented Hybrid Designs

Numerous applications of hybrid actuators have been reported. Some examples include the development of a rotary knob for in-vehicle control [9][10], the combination of an electro-rheological brake and an ultrasonic motor [11], a surgical device with haptic feedback [12], an external knee joint for a rehabilitation device [13], and actuators for telerobotics systems [14].

An and Kwon [15] demonstrated that a motor/brake actuator allows for the simulation of virtual walls without the stability issues observed when using high torque motors only. They also showed in [16] that the maximum simulated stiffness by the motor, for which one can guarantee passivity, can be improved if the brake generates a controllable physical damping. In [17], the reference torque is shared between the actuators and the participation of the brake is increased if instability cycles are detected.

From the control perspective, the reported control methods fall into two categories. 1) While the motor displays reflecting forces, the brake can generate a controllable physical damping in order to respect the stability criterion of (1) [18]. 2) While the brake creates the desired forces, the motor can compensate for the inherent friction introduced by the brake [19]. The first method can render stiffer environments as compared to only using a motor. However, the maximum available torque is the torque capability of the motor. In the second case, the system cannot restore energy to the user. Though, these two control methods turn out to be complementary.

From the mechanical perspective, several ways to link brakes and motors can be envisaged as summarized in Fig. 2. In the schematic, a rectangle, a coil and a piston represent an inertia, a spring and a damper respectively. A motor is illustrated by two parallel lines and a brake by a concave line. A mechanical connection using a continuous line points out a common velocity on each side while connections with dashed lines indicate opposed velocity on each side. Half parallel lines or half concave lines symbolise an actuator that can apply a torque only in one rotational direction.

Arrangement **(a)** is the standard configuration where the brake and the motor are connected in parallel [9] [13] [15] [16] [17] [19] [20] . The torque of each actuator can be combined to create resistive forces. However, if the device restores energy the brake can block the motor and the system behaves as passive.

Option **(b)** is a micro/macro manipulator concept where the brake and the motor are linked in series. The brake actuates as a clutch transferring the motor's torque to the end-effector [14]. For instance, if an ultrasonic motor (USM) is used, thanks to its high blocking torque, the brake can impose a resistive force when the motor is turned off [11]. This option impairs the system to combine the brake/motor torques at the same time.

Configuration **(c)** is a variation of series elastic actuators. The motor and the brake are linked via an angular spring so that the energy provided by the operator can be stored in the spring [21]. The motor compensates for the error between the reference torque and the torque of the spring. In the same way, option **(d)** couples two stages with a viscous damper [5]. The output torque can be controlled by varying the damping coefficient [22].

Alternatively, **(e)** has two brakes acting like clutches that are being driven at same velocity but in opposite directions by

a motor. The brake's outputs are connected in parallel [23]. Each brake transfers the motor's torque to the end-effector in a different direction. When using a USM as power source, the system is equivalent to **(b)**.

In **(f)** two opposite overrunning clutches are mounted on a common shaft. Each of them is connected to a motor. Depending on the relative velocity of the motor and shaft, the shaft is or is not blocked in one direction. Therefore, each motor can restrict the motion of the end-effector only in one direction and cannot directly drive the shaft [24].

Passive actuators are widely used in haptic devices. For instance, a miniature 1-DOF haptic interface based on a magnetorheological (MR) fluid, which produces a torque from 0.03 Nm to 1.7 Nm and consumes 27 Watts in shown in [25] . Compared to a commercial DC motor (Maxon RE25), it represents 51 times more torque for the same volume. A haptic glove, proposed by Blake *et al*. [26], possesses six compact MR brakes which generate a haptic feedback in three fingers, allowing the operator to pick up and feel virtual objects. Lozada *et al*. [27] used MR actuators for haptic feedback in musical keyboards. Other applications of MR fluid include the design of a joystick for virtual reality [28], and rotary knobs for in-vehicle control [29].

2.1 Discussion

Exploring both actuators to simulate stiffness implies using solution **(a)**. In this configuration, the brake can block the motor as exemplified in Fig. 3. In the example the brake and the motor apply the forces F_b and F_m respectively. Consider the simulation of a 1-DOF virtual spring shown in Fig. 3(a). The operator imposes the force F_z to compress the spring (I). The device will react with the force $F_h = F_b + F_m$ that is proportional to the displacement (II). According to Karnopp's model [30], when the brake is commanded to generate a force F_{ref}, the braking force F_b is:

$$F_b = -\min(|F_e|, |F_{ref}|) \begin{cases} \text{sgn}(\dot{x}) & if \quad \dot{x} \neq 0 \\ \text{sgn}(F_e) & if \quad \dot{x} = 0 \end{cases} \qquad (2)$$

where F_e is the external force acting on the brake and $\dot{x}$ is the velocity. In the example, $F_e = F_z - F_m$ and $F_{ref} \geq F_m$. Consequently, when the user releases the handle ($F_z = 0$), the braking force becomes $F_b = -F_m$ (III). The resultant force is zero and handle stays in the compressed position.

Fig. 3(b) shows the simulation of a virtual wall. In (I) the operator applies the force F_z towards the wall. When the end-effector reaches the wall, the device imposes $F_h = F_b + F_m$ against the velocity $\dot{x}$. According to (2), the braking force is always opposed to the operator's force. When the operator inverses the force to come back out of the wall, the braking force is $F_b = -F_z + F_m$. The brake "sticks" the end-effector on the wall even though it should move freely in the direction of $-\dot{x}$ (III) [8].

These drawbacks are avoided if the braking torque becomes zero when the operator reverses motion. In this paper, this is achieved using two unidirectional brakes. This actuation concept is explained in the following section.

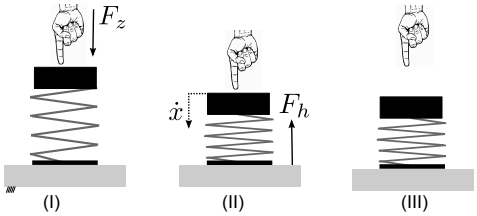

(a) Simulation of a virtual spring

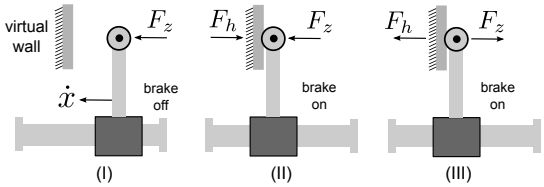

(b) Stickly wall effect using passive actuators

Fig. 3. Simulation of a virtual spring with a motor/brake parallel actuator. In 3(a) the operator applies a force F_z to compress the spring (I) inducing the velocity $\dot{x}$. The device reacts with the force F_h (II). When he releases the handle (III), the brake blocks the motor. In 3(b) the operator moves the handle towards $\dot{x}$ (I), when it reaches the virtual wall the brake applies a resistive force (II) that is always opposed to F_z (III).

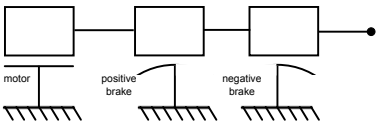

Fig. 4. Working principle of the unidirectional brake based actuator. The brakes are mounted on the shaft through overrunning clutches. The positive brake can only impose a torque if the velocity of the shaft is negative, and the negative brake only if the velocity is positive. The motor applies a torque in both directions.

3. Dual Brake-based Actuation

The proposed actuation concept is based on the combination of options **(f)** and **(e)** with an attempt to obtain an equivalent system to **(a)**. The actuator is composed of two unidirectional brakes and a motor as illustrated in Fig. 4. The brakes are connected to the shaft using overrunning clutches. Thus, they can apply a torque only in one defined rotational direction, while the motor can apply a torque in both directions [31].

Let us say that the positive brake is able to generate a torque Γ_{bp} when the velocity of the shaft $\dot{\theta}$ is negative, and the negative brake can impose a torque Γ_{bn} when the velocity is positive. As a function of the desired torque Γ_h, the selection of the brake is realised as follows:

$$\begin{bmatrix} \Gamma_{bp} & \Gamma_{bn} \end{bmatrix} = \begin{cases} \begin{bmatrix} \Gamma_h & 0 \end{bmatrix} & \Gamma_h < 0 \\ \begin{bmatrix} 0 & \Gamma_h \end{bmatrix} & \Gamma_h > 0 \end{cases} \qquad (3)$$

Fig. 5 shows the torque capability of the system. When $\text{sgn}(\Gamma_h) \neq \text{sgn}(\dot{\theta})$, the total torque is the contribution of the brake and the motor (Γ_m), otherwise only the motor can provide a torque. Thanks to the overrunning clutches, the brakes provide torques only if the velocity is opposed to the reference torque. Both brakes are be released if $\Gamma_h = 0$.

Consider the implementation of this actuator in the examples of Fig. 3. The brake able to generate a torque in the direction of the reference force is activated. In the simulation

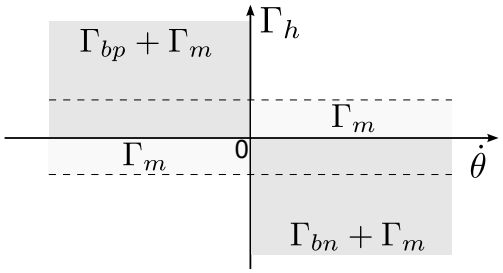

Fig. 5. Torque capability the actuator. Γ_m, Γ_{bp}, and Γ_{bn} are the torque provided by the motor, by the positive and by the negative brake respectivelly. $\dot{\theta}$ is the velocity and is Γ_h is the desired torque.

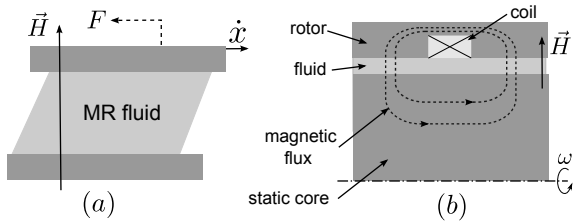

Fig. 6. MR fluid suspension in shear mode. The fluid is confined between two magnetic poles. In (a) the field $\vec{H}$ dependent force F is applied against the velocity $\dot{x}$. In (b) the working principle of a rotary brake. A coil generates a magnetic flux applied perpendicular to the shear surface. The fluid resits against the velocity ω.

of the virtual spring, the braking torque becomes zero if the operator releases the handle. Therefore, the motor can simulate the decompression of the spring. In the simulation of the virtual wall, if the operator reverses motion, only the motor provides a torque and it can repulse the end-effector out of the wall.

The following section presents the mechanical design of this system and the development of the associated control laws.

4. Design of The Hybrid Actuator

The passive actuator adopted in this research is a magnetorheological (MR) brake. An MR fluid is composed of soft micrometric ferromagnetic particles dispersed in a carrying liquid. Its rheological properties can be strongly and reversibly modified by the action of a magnetic field [32]. The magnetisation of the particles engenders the formation of chain-like structures aligned roughly parallel to the magnetic field. By controlling the magnetic field intensity, an MR fluid can achieve a wide range of apparent viscosity . The yield stress can attain 100 kPa with relatively low operating currents and voltages, making MR fluids particularly suitable in the design of human-machine interfaces.

The working principle of MR brakes is presented in Fig. 6(a). The fluid is confined between two magnetic poles. The chain-like structures create a resistive force F against the relative velocity $\dot{x}$ of the poles. This force depends on the applied field $\vec{H}$. Fig. 6(b) shows a rotary brake. The magnetic field is provided by a coil to control the resistance against the rotor velocity ω.

4.1 Magnetomechanical Design

A CAD cross view of the actuator is shown in Fig. 7. The motor (Maxon RE40-1148877) is directly connected to the through-axis. Two identical brakes associated to an overrunning clutch[1] are mounted on the same shaft. A brake is composed of the following parts. The overrunning clutch is mounted on the axis in a rotary cylinder (A). Over this cylinder, a thin non-magnetic disc (B) is connected to support in its upper extremity two ferromagnetic cylinders (C). The assembly A-B-C rotates only of the velocity of the shaft is negative, otherwise this rotation is not transferred to these parts. The coil is built in the static ferromagnetic path (D). A static ferromagnetic cylinder (E) is connected to it in order to form the fluid chamber. The fluid is spread all over the 4 equidistant gaps. The sealing is ensured using low-friction rubber radial shaft seals without spring compressors. The position of the shaft is measured with a 500 pulse per revolution incremental encoder.

The behaviour of MR fluids as a function of a magnetic field H can be described by the Bingham model. This formulation yields:

$$\tau(\dot{\gamma},H) = |\tau_y(H)| + |\dot{\gamma}|\eta \tag{4}$$

where $\dot{\gamma}$ is the fluid shear rate, η the viscosity coefficient and $\tau_y(H)$ the field dependent yield stress. The field dependent torque $\Gamma_n(H)$ delivered by a cylinder n is obtained as the integral of the field dependent yield stress $\tau_y(H)$ over the shear surface S_n that has a radius r_n as:

$$\Gamma_n(H) = \int\int_{S_n} r_n \tau_y(H) dS_n \tag{5}$$

Before saturation of the fluid, the yield stress can be considered a linear function of the magnetic field H [25], and H proportional to the magnetic flux density B. Thereby, the relation $\tau_y = \alpha B/\mu_{mr}$ can be established where α is a fluid constant and μ_{mr} is the fluid absolute permeability. Considering only the magnetic reluctance of the fluid, (5) can be rewritten as:

$$\Gamma_n(H) = \int\int_{S_n} r_n \frac{\alpha}{\mu_{mr}} |B(u)| du \tag{6}$$

The torque for m fluid gaps is obtained as the sum of the torque of each shearing surface as:

$$\Gamma(H) = 2\pi \frac{\alpha}{\mu_{mr}} \sum_{n=1}^{n=m} r_n^2 \int_0^h |B(u)| du \tag{7}$$

where h is the fluid gap width.

The minimum required controllable braking torque is 3.2 Nm. This corresponds to the maximum average torque exertion of the human hand using a circular shaped handle with a diameter comprised 30mm and 35mm [33][34]. The maximum outer diameter is set to 60 mm, and a the hollow shaft has 12 mm diameter. The fluid gap depth was set to 0.5 mm.

The fluid is Lord Corporation MRF122EG. In order to avoid saturation, the induction of the fluid and of the ferromagnetic

[1] http://uk.misumi-ec.com/eu/ItemDetail/10302273810.html

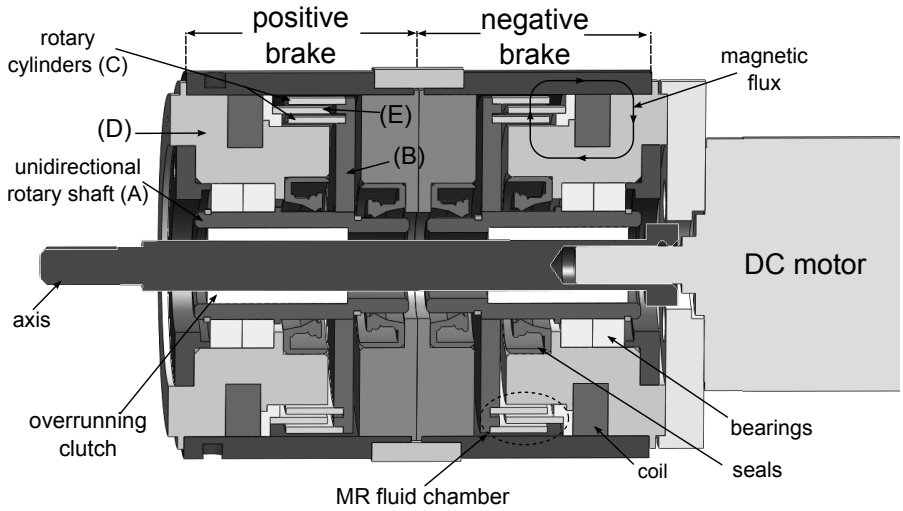

Fig. 7. CAD view of the hybrid actuator. Two identical magnetorheological brakes are mounted on the motor's shaft through overrunning clutches. The assembly A-B-C is the rotary part. A coil is made in the ferromagnetic static part D in order to generate the magnetic flux across the four equidistant fluid gaps.

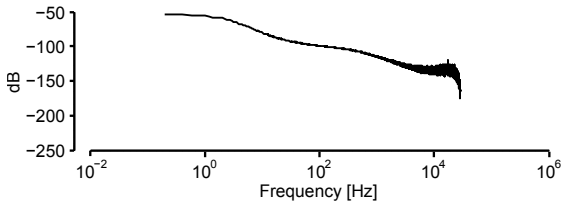

(a) Voltage to current gain

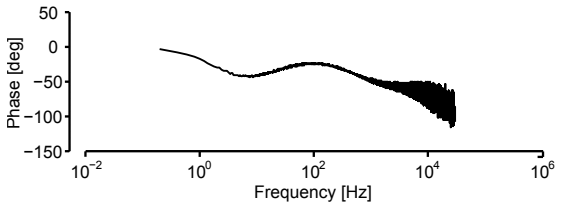

(b) Voltage to current phase

Fig. 8. Electromagnetic frequencial respose of the brake. A 10 s sinusoidal sweep frequency of a 12 V varing from 0.1 Hz to 30 kHz is sent to the brake and the current is measured by a shunt resistance of 1 Ω. The observed cut-off frequency is 18 Hz.

path must not exceed 0.7 T and 1.7 T respectively. Thus, the magnetic circuit and the coil are designed to provide the required torque when the *smallest* fluid surface reaches 0.7 T. The complete modelling approach is fully described in [35] and [36]. After optimisation using finite element analysis, four fluid gaps were obtained. Each one is 7 mm in length, with a 22.5 mm, 24 mm, 25.5 mm and 27 mm radius respectively. The assembly comprising the two brakes has a 78 mm width.

From these results, the desired induction requires a coil with 232 AT. It is achieved using 475 turns of a 0.25 mm diameter copper wire and 0.49 A, which corresponds to the nominal operating range of the brake. When exploited beyond this point, the fluid becomes gradually saturated. The complete saturation is considered as the point where the *largest* fluid surface reaches 0.7 T at 0.9 A.

4.2 Characterization

The assembled actuator was mounted in the test bench schematized in Fig. 9. A DC RE40 50:1 geared Maxon motor is used as a torque source. The motor is connected to the actuator through a Sensor Development 01324 torque transducer. The current of the brakes is controlled by a custom made analog proportional-integral (PI) controller.

The excitation motor is activated with a slow velocity and a current with a triangular wave form is sent to the brakes to obtain their magnetic hysteresis loops as presented in Fig. 10. The current starts from 0 A and is constantly increased by 1 mA each 10 ms up to 0.9 A, and then decreased up to zero again. The measured braking torque at 0.49 A is 3.6 Nm. This result exceeds the analytical model by 5.5%. The maximum braking torque measured at the complete saturation of the fluid is 5.3 Nm.

The magnetic hysteresis shown in the experimental results can be compensated using nonlinear functions to fit the sub-hysteresis loop [28]. We consider here only the first subhysteresis loops (increasing torque). The torque as a function of the current i can then be approximate by:

$$\begin{bmatrix} \Gamma_{bp} \\ \Gamma_{bn} \end{bmatrix} = \begin{cases} \begin{bmatrix} 6.96i \\ 6.55i \end{bmatrix} & 0 \leq i \leq 0.61A \\ \begin{bmatrix} 3.25i + 2.26 \\ 4.13i + 1.47 \end{bmatrix} & 0.61A < i \leq 0.92A \end{cases} \tag{8}$$

Each coil possesses an electrical resistance of 24 Ω. The electrical response of the coil is presented in Fig. 8. The bode diagram is obtained using a 12 V excitation sinusoidal voltage of with a sweep frequency from 0.1 Hz to 30 kHz. The induced current is measured with a shunt resistance of 1 Ω. The observed cut-off frequency at $\pi/4$ rad out of phase is 18 Hz. The measured electromechanical response time for a step voltage excitation is 200 ms. By controlling the closed loop current in with the PI controller, the response time is 30 ms.

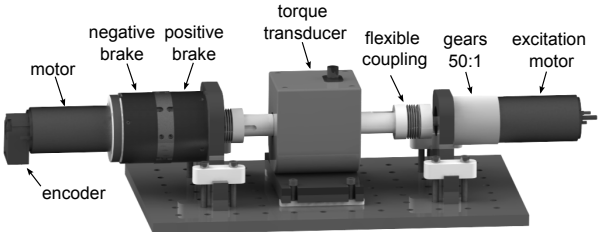

Fig. 9. Test bench used for characterization. A 50:1 geared RE40 Maxon motor is used as torque source. The current sent to the brakes is controlled using an analog PI controller.

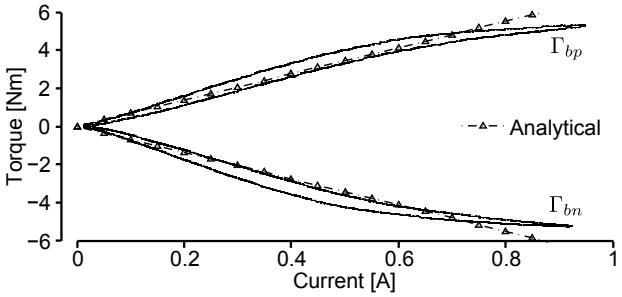

Fig. 10. Measured braking torque. A triangular current slop is sent to the brakes during rotation. The maximal measured torque is 5.3 Nm at 0.9 A.

The no load current of the hybrid actuator, when only the motor is activated, is $i = 2.23$ A. Given the motor's torque constant $k_i = 60.3\times10^{-3}$ Nm A^{-1}, this represents a no load torque given by $i_0 \times k_i$ of 0.134 Nm. The attained velocity in this case is $\omega_0 = 182$ rad s^{-1}. The estimated viscous torque coefficient $b = i_0 k_i \omega_0^{-1}$ then is 732×10^{-6} Nms. Using the same torque/velocity step response, the inertia of the hybrid system was calculated and the result corresponds to the CAD model. The estimated rotor inertia is 418 gcm^2.

4.3 Performance evaluation

The performance of the hybrid actuator are compared to the characteristics of the motor, and of the motor associated to an ideal reduction stage which is a common architecture of several haptic devices.

In its recommended operating range the motor's nominal torque is 0.2 Nm, thus the maximum torque of the hybrid actuator is 5.5 Nm. To achieve this torque without brakes, the motor would need to have a 27.5:1 reduction ratio. For comparison purposes, consider an hypothetical ideal capstan transmission which has no inertia, no friction and no mechanical losses.

According to the motor datasheet, the no load current is 69 mA and the torque constant is 60.3×10^{-3} Nm A^{-1}. This corresponds to an off-state torque of 4.16×10^{-3} Nm. The no load velocity of the motor is 793 rad s^{-1}, it yields a viscous torque coefficient of 5.24×10^{-6} Nm s. The inertia of the motor is 134 gcm^2.

The performance of the motor, of the motor with capstan transmission, of a single brake and of the hybrid actuator are listed in Table I. The characteristics of a EC motor which has the same diameter as the hybrid actuator is also included for reference. Each brake has a torque density of 48 kNm^{-2} and consumes 20 W. Compared to the motor, a brake and the hybrid actuator have a torque density 21 and 7.9 times greater than the motor respectively.

Compared to the hybrid actuator, the motor with capstan has 241 times more inertia, 3.35 times more off-state torque but generates 5 times less viscous torque for a given velocity. The necessary rotational velocity to reach the same viscous plus off-state torque in both devices is 142 rad s^{-1}. In other words, the hybrid actuator generates less frictional torques than the motor with capstan up to 1362 rpm. Velocities around this value are rarely observed in haptic interactions.

This low response time has a strong influence on the stiffness simulated by the brakes called K_b. Considering r the number of pulses-per-revolution of the position encoder, the minimum detectable position variation is $d\theta = 2\pi/4r$ radians and the position variation during the leading edge pulsing time of the brake is $\delta t\,\omega(t)$, where δt is the response time of the brake. The maximal perceived stiffness by the operator is:

$$K_b = \begin{cases} \frac{\Gamma}{\delta t \dot{\theta}} & if \quad \omega(t) > \frac{d\theta}{\delta t} \\ \frac{\Gamma}{d\theta} & otherwise \end{cases} \tag{9}$$

Using an incremental encoder with $r = 500$, the maximal displayable stiffness is 1687 Nm rad^{-1} for interaction velocities up to 0.1 rad s^{-1}.

This evidence demonstrates that the hybrid actuator has less inertia and friction compared to a motor with ideal capstan system. When dissipating energy, the hybrid actuator can provide 5.5 Nm, however, different to the motor with capstan, the hybrid actuator can apply only 0.2 Nm when restoring energy.

TABLE I
COMPARISON WITH A COMMERCIAL MOTOR

	unit	Maxon RE40	Maxon EC60	RE40 capstan	Single brake	Hybrid actuator
Passive Torq	Nm	0.2	0.83	5.5	5.3	5.5
Active Torq	Nm	0.2	0.83	5.5	0	0.2
Reduc. ratio	-	1	1	27.5	1	1
Power	W	150	400	150	20	170
Inertia	gcm^2	134	831	101k	279	418
Visc. Coef.	μNms	5.24	137	144	567	732
Min torque	Nm	0.004	0.044	0.114	0.03	0.034
Max/min T	-	48	18.8	48	176	161
Torq/v.coef	ms^{-1}	38.16	6.05	38.16	9.34	7.51
Torq/inertia	N/gm	14.9	9.98	0.54	189	131
Torq/vol	kNm^{-2}	2.24	7.1	-	48.1	17.75

5. HYBRID ACTUATOR CONTROL

In this second part of the paper, the control laws are addressed. Two algorithms are proposed. The first one limits the stiffness displayed by the motor and uses the motor/brake combination to respect a reference torque. The second algorithm bounds the interaction energy to no more than the energy provided by the operator. The first requirement for the controller is to decouple the design of the controller from that of the virtual environment. The brake and the motor are considered as two independent systems. The proposed control laws are based on the following four premises: 1) The controller only knows the position and the desired torque; 2) the stiffness simulated by the motor is bounded to avoid

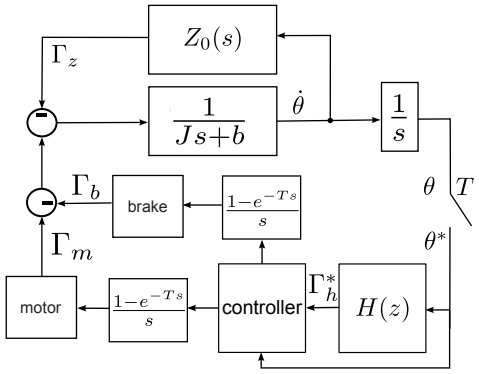

Fig. 11. Control scheme of an hypothetical brake/motor interface. The device has an inertia J and a friction b. The torque applied by the brake, by the motor, and by the operator are Γ_b, Γ_m and Γ_z. The operator acts as a passive impedance $Z_0(s)$. The virtual environment $H(z)$ calculates the reference torque Γ_h^* as a function of the measured position θ^*. A discrete controller calculates the torque for both actuators. Variables marked with an asterisk are discrete variables and $(1-e^{-Ts})s^{-1}$ is the zero-horder hold function with has a sampling rate T.

instability; 3) the interaction's energy is bounded to respect passivity; and 4) the participation of the motor is maximized to compensate for the response time of the brakes.

In the following, consider the hypothetical hybrid haptic device shown in Fig. 11. The device has inertia J and damping b. The operator is the passive impedance $Z_0(s)$ and he applies a torque Γ_z. The velocity is called $\dot{\theta}$. The virtual environment is the discrete function $H(z)$, linear or not, which calculates the reference torque Γ_h^* as a function of the position θ^*. The asterisk identifies variables in the discrete domain. The transition from the discrete to the continuous domain is given by the zero-order hold function $ZOH(s) = (1-e^{-sT})s^{-1}$ according to a sample period T. Using only the position and the reference torque, the controller calculates the brake torque Γ_b and the motor torque Γ_m.

5.1 Stiffness Bounding

Considering the simulation of a virtual wall with no damping, the maximum stiffness for which one can guarantee passivity called K_{lim} is given by (1) for $B = 0$ so that $K_{lim} \leq 2b/T$. Note however, that the controller does not need to have a prior knowledge about the virtual environment. A maximum torque per position variation can be attributed to K_{lim}. This algorithm ensures that this value is not exceeded to avoid instability regardless of the virtual environment model.

The controller compares the variation of the reference torque Γ_h^* with the current torque provided by the motor Γ_{sb}^* in order to deduce the requested stiffness K_h. If $K_h > K_{lim}$, then Γ_{sb}^* is recalculated. The difference $\Gamma_h^* - \Gamma_{sb}^*$ is supplied by the brake. The stiffness observer is:

$$K_h = \frac{\Gamma^*_{h(k)} - \Gamma^*_{sb(k-1)}}{\theta^*_{(k)} - \theta^*_{(k-1)}} \tag{10}$$

where the index (k) represents the current value of the variable and $(k-1)$ is the value at the previous sampling instance. The maximum torque that can be sent to the motor is:

$$\Gamma^*_{sb(k)} = \begin{cases} \Gamma^*_{h(k)} & if \quad K_h \leq k_{lim} \\ K_{lim}(\theta^*_{(k)} - \theta^*_{(k-1)}) + \Gamma^*_{sb(k-1)} & otherwise \end{cases} \tag{11}$$

Considering Γ_{sat} the torque capability of the motor, the fraction of the reference torque that can be delivered by the motor, called $\beta(\Gamma_h^*)$, is:

$$\beta(\Gamma_h^*) = \frac{\min\left(\left|\Gamma_{sb}^*\right|, \left|\Gamma_{sat}\right|\right)}{\left|\Gamma_h^*\right|} \tag{12}$$

so when $\beta(\Gamma_h^*) = 1$ that all the reference torque can be assumed by the motor. For $0 < \beta(\Gamma_h^*) < 1$, the motor is physically saturated or its torque is bounded by the controller. In this case, the difference should be sent to the brake.

Finally, the reference torque sent to the motor is $\Gamma_m^* = \Gamma_h^* \beta(\Gamma_h^*)$ and the braking torque is $\Gamma_b^* = \Gamma_h^* - \Gamma_m^*$, or rather $\Gamma_b^* = \Gamma_h^*(1 - \beta(\Gamma_h^*))$. This formulation implies that Γ_h^* is initially transferred to the motor and thereby its participation is maximized.

5.2 Energy Bounding

In the stiffness bounding algorithm, if either K_{lim} or K_h are missestimated, the stability is not ensured. Hence, a second algorithm is proposed to guarantee the passivity if the first algorithms fails. A complementary function of this algorithm is to turn the brakes off when the interface restores energy.

The instantaneous behaviour of the system (passive or active) can be determined by the interaction power P. The observed power is $P = \dot{\theta}^* \left[-\Gamma_m^* - \Gamma_b^*\right]$ where the measured velocity is $\dot{\theta}^* = \theta^*(1-z)/Tz$. Assuming that $\Gamma_h = \Gamma_m + \Gamma_b$, the power can be rewritten as $P = (-\Gamma_h^*)\dot{\theta}^*$ [8]. Positive power indicates that the interface dissipates energy. Conversely, negative power indicates an active behaviour and brakes can be turned off [37].

A power-sign dependent variable $\sigma(P) = 0$ if $P \geq 0$ and $\sigma(P) = 1$ if $P < 0$, is defined as follows :

$$\sigma(P) = \frac{1}{2}\left[\mathrm{sgn}(P) - 1\right]\mathrm{sgn}(P) \tag{13}$$

A statement of passivity is that the energy in the device is never greater than the energy provided by the operator [38] [39]. The energy of the motor is $E(n) = -\sum_{k=1}^{n} \Gamma_m(k)\dot{\theta}(k)$. If this energy becomes negative, the interface is not passive. The created energy $-E(n)$ needs to be dissipated and the reference torque Γ_h^* is transferred to the brake instead of the motor.

The energy observer $E_o(n)$ is defined as a function of the torque provided by the motor and the energy dissipated in the brake as:

$$E_o(n) = -\sum_{k=1}^{n} \left[\Gamma_m(k) + \Gamma_b(k)\sigma(P)\right]\dot{\theta}(k) \tag{14}$$

As long as $E_o(n) < 0$, two possibilities come up: 1) If the operator turns the end-effector in the direction of the reference torque ($P < 0$) the brake is activated to dissipated the energy while $E_o(n) \geq 0$; 2) If the operator turns the end-effector in the opposite direction ($P > 0$), the motor can again be activated.

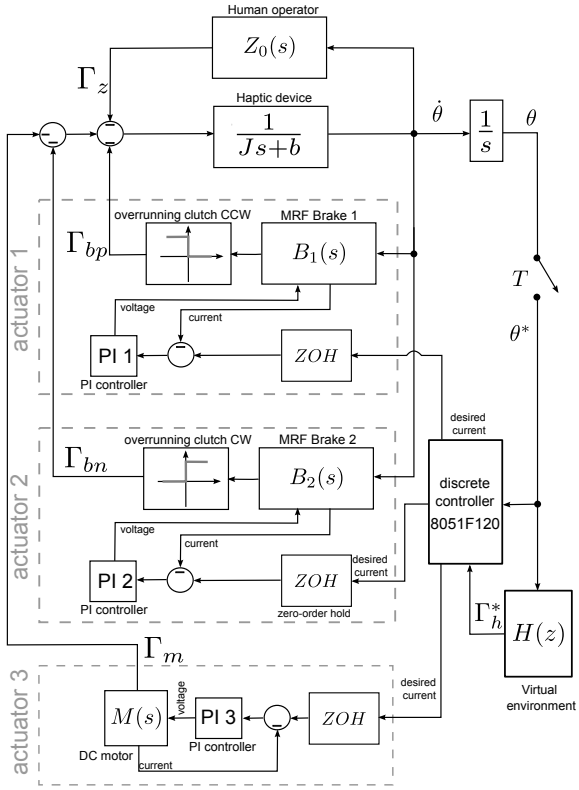

Fig. 12. Block diagram of the haptic device. The device has an inertia J and a damping b. The operator $Z_0(s)$ applies a torque Γ_z. The torque of the motor, and of the brakes are called Γ_m^*, Γ_{bp}, and Γ_{bn}. The virtual environment $H(z)$ calculates the desired torque Γ_h^* as a function of the position θ^*. The position is sent to the controller that determines the torques of each actuator. The asterisk represents discrete. *ZOH* is obtained a zero-order hold function with a sample rate $T = 200$ μs. The current sent of each actuator is controlled with an analog proportional-integral controller (PI). The electromechanical transfer function of the motor and of each brake are called $M(s)$, $B_1(s)$ and $B_2(s)$.

The control variable $S(n)$ is then introduced to determine the sharing of Γ_h^* into Γ_b^* and Γ_m^* so that: if $S(u) = 1$ only the motor is enabled; if $0 < S(n) < 1$, the reference torque is applied using both actuators. Taking into consideration the limitation of the stiffness, $S(n)$ takes the following formulation:

$$S(n) = \begin{cases} \beta(\Gamma_h)(1-\sigma(P)) + \sigma(P) & if \quad E_o(n) \geq 0 \\ \beta(\Gamma_h)(1-\sigma(P)) & otherwise \end{cases} \quad (15)$$

The torque provided by the motor then is $\Gamma_m = ZOH[\Gamma_h^* S(n)]$, and the braking torque is $\Gamma_b^* = \Gamma_h^*(1 - S(n))$. The torque of each brake is obtained by rewriting (3) as $\Gamma_{bp} = ZOH[\Gamma_b^*]$ and $\Gamma_{bn} = 0$ if $\Gamma_h^* > 0$ and $\Gamma_{bn} = ZOH[\Gamma_b^*]$ with $\Gamma_{bp} = 0$ if $\Gamma_b^* < 0$.

6. Simulation of Helical Springs

An overview of the hybrid interface control-loop is shown in Fig. 12. Each overrunning clutch is modelled as an unilateral constraint. The brake 1 and the brake 2 apply the torques Γ_{bp} and Γ_{bn} respectively. The brake is modelled as a transfer function $B(s)$ and the motor as the transfer function $M(s)$. A voltage is applied by on each actuator and the current in monitored by the PI controllers. The reference torque is $\Gamma_h^* = H(z)\theta^*$. The system is operated by a Scilabs 8051F120 microcontroller running at a sample period T of 200 μs. Note that the control scheme is independent of the virtual environment.

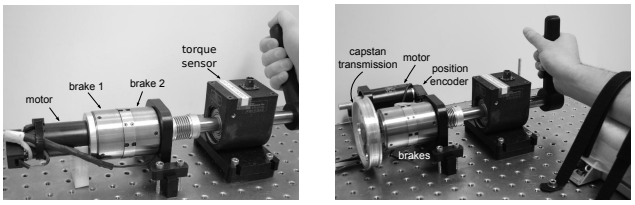

(a) motor without reduction (b) motor with capstan

Fig. 13. Experimental setups. In Fig. 13(a) the motor is directly connected to brakes, in Fig. 13(b) a 7:1 capstan transmission is used.

The experimental setup is shown in Fig. 13(a). A 200 mm handle is connected to the actuator through a torque transducer. The virtual environment is defined as virtual springs so that $H(z) = K_h$, where K_h is its stiffness. The maximum stiffness supported by the motor is set to $K_{lim} = 6.8$ Nm rad^{-1}. Two tests are presented i.e. $K_h >> K_{lim}$ and $K_h = K_{lim}$.

Fig. 14 shows the simulation of a 60 Nm rad^{-1} virtual spring. The operator turns the handle in order to compress the spring which is placed at 0.05 rad. The torque is calculated by virtual environment and sent to the controller. At the initial contact, because $K_h >> K_{lim}$, the torque sent to the motor is bounded so that the simulated stiffness is less than or equal to 6.8 Nm rad^{-1}. Since the motor can ensure only 11% of the total torque, the difference is sent to the brake which displays 53.2 Nm rad^{-1}. When the motor reaches its maximum torque at the point (A), the stiffness sent to the brake increases to 60 Nm rad^{-1}. Viscous and coulomb frictions are not compensated.

Fig. 15 presents the simulation of a 6.8 Nm rad^{-1} virtual spring. Since $K_h \leq K_{lim}$, the reference torque can be provided by the motor ($\beta = 1$). When the motor reaches its maximum torque $\Gamma_{sat} = 0.2$ Nm the difference between the reference torque and the maximum motor's torque is compensated by the brake. At the point (A) the operator reverses the motion. The velocity is in the direction of the reference torque and the brake is turned off. From this point only the motor remains activated providing a small amount of the torque as the position continues to decrease. This is the major difficulty in representing elastic elements using the proposed device. The area marked by W corresponds to the mechanical work that cannot be restored.

The major limitation of the proposed device is the simulation of compliant elastic elements, as the motor can provide only a small amount of torque compared to the brake. In the next section, a second experiment is performed in order to evaluate the influence of this asymmetry on the perception of elasticity. The objective is to observe and quantify the operator's capability detecting the drop in torque when they reserve motion.

6.1 Perceptual Evalulation of Torque Asymmetry

In this experiment the operators interact with soft virtual springs. The participant was seated in front of the device and

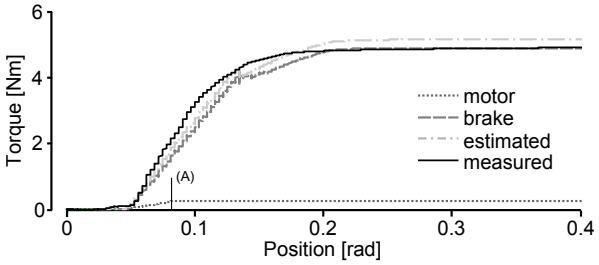

(a) Torque

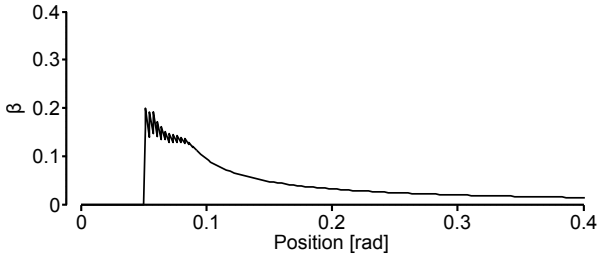

(b) Torque sharing coefficient

Fig. 14. Simulation of a 60 Nm rad^{-1} virtual spring. The torque sent to the motor is bounded to its maximum stiffness of 6.8 Nm/rad. The difference, 53.2 Nm/rad is sent to brake up to the saturation of the motor (A). Before the saturation $\beta = 6.8/60$ and after it $\beta \to 0$. Then, all the reference stiffness is sent to the brake.

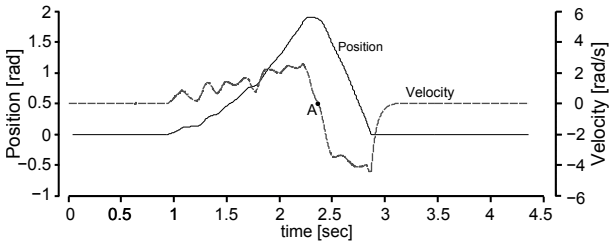

(a) Position and velocity

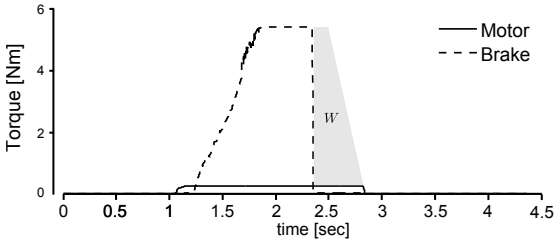

(b) Torque

Fig. 15. Simulation of a 6.8 Nm rad^{-1} virtual spring. The end-effector attains the spring at 1.1 s (15(a)). Initially, all of the reference torque can created by the motor. The brake is activated when the motor reaches its maximum torque. At the point A (15(b)) the operator reverses the motion and the brake is turned off.

his front arm was stabilized on the mount so that his hand clasps the handle in the vertical position. The motor is linked to the brakes through a 1:7 capstan transmission as shown in Fig. 13(b). Both the maximum motor's and brake's torques are limited to 1.2 Nm. The participation of the motor is then controlled and operators were requested to interact with the springs and identify whether it reacted with the same torque or stiffness during both compression and decompression phases.

Two different stiffness K_h (4.5 and 2.9 Nm rad^{-1}), and two maximal displacements θ_{max} (30° and 15°) are assigned to the springs. Thus, four different scenarios were composed. In the following, *symmetry ratio* defines the percentage of K_h simulated by the motor, or the percentage of the total torque $K_h \times \theta_{max}$ delivered by the motor at the maximum displacement.

Environments: Two different environments were used: (1) The stiffness simulated by the motor is bounded by setting $K_{lim} < K_h$. Thus, during the compression phase, the spring can be stiffer than during the decompression phase (see Fig. 16(a), left). (2) The maximum torque of the motor is limited by Γ_{sat} (see Fig. 16(b), left). For each environment, there are eleven symmetry ratios ranging from 0% (i.e. $K_{lim}/K_h = 0$ or $\Gamma_{sat} = 0$, only the brake is used) to 100% (only the motor is used).

Participants: 17 participants (4F, 13M) aged from 21 to 32, (average age of 23 years) participated in the experiments. None of them had prior knowledge about the device workings. They were divided into two different groups of 9 and 8 participants. The first group realized tests with asymmetric stiffness environments and the second group with torque asymmetric torque environments.

Procedure: The haptic device was hidden and the participants had no visual feedback of their actions. Each participant was allowed to get acquainted with the device by interacting as long as he desired with virtual environments with known scenarios and symmetry ratio. Each participant realized 110 manipulations for each scenario determined randomly. Thus, each asymmetry level was presented 10 times within each scenario.

For each manipulation, a symmetry ratio was randomly assigned to the virtual environment. Subjects were instructed to firmly hold the end-effector and to compress the virtual spring and then return to the initial position. Three degrees before the respective end position, a buzzer sounded. The end position θ_{max} was indicated by a second buzzer. The participants were instructed to turn the handle back before the second signal. They were allowed to compress and decompress the virtual spring at most two times. After each manipulation, the participants were asked to classify the environment as symmetrical (same stiffness or torque during both phases) or asymmetrical.

Fig. 16(a) (right) shows the average rate of manipulations perceived by the participants as symmetric for all scenarios, as a function of the stiffness symmetry ratio. The results demonstrated that for symmetry levels less than 50%, participants perceived the torque in 80% of the manipulations. Conversely, for manipulations with a symmetry ratio higher than 80%, on average, the operator did not perceive the torque drop in

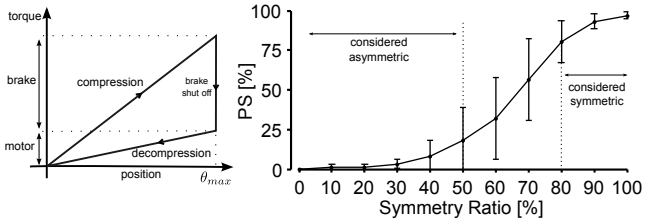

(a) Stiffness limitation

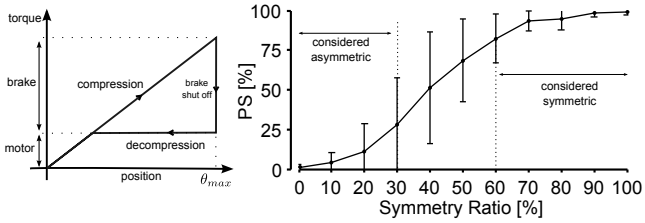

(b) Maximum torque limitation

Fig. 16. Experimental results for stiffness and torque limitations. The ratio of stimuli perceived as symmetric (PS) as function of the symmetry ratio (right). The symmetry ratio is the level of participation of the motor in the desired stiffness or maximum torque (left).

80% of the manipulations. The results are equivalent for all scenarios. Participants were able to base the discrimination on two aspects, i.e. the torque perceived when they reversed motion, or the torque close to the initial position. For low symmetry ratio, the initial force could be very low and may become imperceptible. Therefore, the participants classified the spring as asymmetrical. This may partly explain the low discrimination threshold of 50%.

Fig. 16(b) (right) shows the average of manipulations perceived as symmetric for all scenarios with torque limitation. For a symmetry ratio less than 30%, participants perceived the torque drop in 80% of the manipulations. Conversely, when the symmetry ratio was higher than 60%, they did not perceive the torque drop in 80% of the manipulation. The asymmetry is due to the limitation of the maximum torque. This means that there is a region where the torques are the same during the compression or decompression phases. For example, considering a symmetry ratio of 50% with $\theta_{max} = 30°$. Up to 15°, the torque in both phases is the same, and only between 15° and 30°, can the asymmetry be observed (see Fig. 16(b), right). In contrast to the previous environments, the observed asymmetry is due to the torque drop only. This may partly explain why the discrimination threshold of 50% and 80% are shifted to 30% and 60%.

These results suggest that operators perceived the asymmetry on the basis of the initial torque rather than on the torque drop when they reversed the motion. The influence of the asymmetry can be minimized by controlling the initial force. In other words, the device does not need to restore exactly the same amount of the provided energy. Note that this experiment is the most unfavourable application case for the proposed device.

7. Conclusion

This paper addressed the development of a hybrid actuator for haptic devices, from modelling to control and evaluation. The actuator has two brakes and a DC motor. A brake has 39 mm width and 30 mm diameter. It can produce a torque from 0.03 Nm to 5.3 Nm, giving a torque density of 48 kNm^{-2} and a maximum-to-minimum torque ratio of 176. The complete system has a torque density 7.9 times higher than the motor. Quantitative results demonstrate that the device exhibits less inertial and frictional torques compared to a motor associated to an ideal capstan transmission.

The use of unidirectional brakes eliminates the sticking effect observed in hybrid actuators when the brake and the motor are linked in parallel. Usually, this is solved using torque or force sensors [15][16][17][19][20] which are bulky and costly, increasing the complexity of the system. However, without torque sensor, friction and non linearities introduced by the brake cannot be directly compensated, and furthermore, the brakes have a high response time. Alternative solutions exist to deal with this limitations.

Erol *et al.* [28] demonstrated that the hysteresis can be eliminated by directly controlling the magnetic field instead of the current using Hall effect sensors. The response time can be reduced by increasing the current per surface ratio in the coil, or by placing the coil closer to the axis [35]. In the same way, viscous friction dramactically drops with the fluid gap depth, at the cost of higher power supply. To reduce Coulomb friction, magnetic seals can replace the current rubber seals as shown in [40]. Alternatively, a technique to detect external torques by monitoring the impedance of the coil presented in [41] can be used in the controller to actively compensate for it using the motor.

The second part of the paper focussed on the associated control laws. The algorithm determines the stiffness of the virtual environment and bounds the torque of the motor in order to limit the simulated stiffness by the motor to no more than a predefined value. The brake is then used to compensate for the difference with regards to the reference torque. Thus, in contrast to related works where either the brake or the motor are used to create the forces [15][19], both actuators are employed using the proposed laws. The interaction energy is bounded to no more than the energy provided by the operator to guarantee the interaction's pasivity if the first algorithm fails. The algorithm does not need any force or torque measurement and is independent of the virtual environment model.

The motor can provide only a small amount of the torque compared to the brakes. The active torque is 27.5 times less than the passive torque. An specific user experiment suggested that the device can give the operator the illusion of elasticity even if only a small amount of torque is available.

The actuator design and its control laws are independent of the virtual environment model allowing for implementation of the device in several haptic feedback interfaces.

References

[1] V. Hayward and O. R. Astley, "Performance measures for haptic interfaces," in *Robotics Research*. Springer, 2000, pp. 195–206.

[2] S. McJunkin, Y. Li, and M. O'Malley, "Human-machine admittance and transparency adaptation in passive user interaction with a haptic interface," in *Eurohaptics Conference, 2005 and Symposium on Haptic Interfaces for Virtual Environment and Teleoperator Systems, 2005. World Haptics 2005. First Joint*, 2005, pp. 283–289.

[3] N. Diolaiti, G. Niemeyer, F. Barbagli, and J. Salisbury, "A criterion for the passivity of haptic devices," in *Robotics and Automation, 2005. ICRA 2005. Proceedings of the 2005 IEEE International Conference on*, april 2005, pp. 2452 – 2457.

[4] J. Colgate and G. Schenkel, "Passivity of a class of sampled-data systems: application to haptic interfaces," in *American Control Conference, 1994*, vol. 3, june-1 july 1994, pp. 3236 – 3240 vol.3.

[5] A. Mohand, G. Millet, S. RÃl'gnier, S. Haliyo, and V. Hayward, "Haptic interface transparency achieved through viscous coupling," *The International Journal of Robotics Research*, vol. 31, no. 3, pp. 319–329, 2012.

[6] O. Baser, E. Konukseven, and H. Gurocak, "Transparency improvement in haptic devices with a torque compensator using motor current," in *Haptics: Perception, Devices, Mobility, and Communication*, ser. Lecture Notes in Computer Science, P. Isokoski and J. Springare, Eds. Springer Berlin / Heidelberg, 2012, vol. 7282, pp. 37–46.

[7] C. Ott, R. Mukherjee, and Y. Nakamura, "Unified impedance and admittance control," in *Robotics and Automation (ICRA), 2010 IEEE International Conference on*, may 2010, pp. 554 –561.

[8] C. Rossa, J. Lozada, and A. Micaelli, "Interaction power flow based control of a 1-dof hybrid haptic interface," in *Haptics: Perception, Devices, Mobility, and Communication*, ser. Lecture Notes in Computer Science, P. Isokoski and J. Springare, Eds. Springer Berlin Heidelberg, 2012, vol. 7283, pp. 151–156.

[9] M. Badescu, C. Wampler, and C. Mavroidis, "Rotary haptic knob for vehicular instrument controls," in *Haptic Interfaces for Virtual Environment and Teleoperator Systems, 2002. HAPTICS 2002. Proceedings. 10th Symposium on*, 2002, pp. 342 –343.

[10] D. Chapuis, X. Michel, R. Gassert, C.-M. Chew, E. Burdet, and H. Bleuler, "A haptic knob with a hybrid ultrasonic motor and powder clutch actuator," in *EuroHaptics Conference, 2007 and Symposium on Haptic Interfaces for Virtual Environment and Teleoperator Systems. World Haptics 2007. Second Joint*, march 2007, pp. 200 –205.

[11] D. Chapuis, R. Gassert, E. Burdet, and H. Bleuler, "Hybrid ultrasonic motor and electrorheological clutch system for mr-compatible haptic rendering," in *Intelligent Robots and Systems, 2006 IEEE/RSJ International Conference on*, oct. 2006, pp. 1553 –1557.

[12] B. Gonenc and H. Gurocak, "Haptic interface with hybrid actuator for virtual needle insertion and tissue cutting," in *Haptics Symposium (HAPTICS), 2012 IEEE*, march 2012, pp. 451 –455.

[13] J. Chen and W.-H. Liao, "Design and testing of assistive knee brace with magnetorheological actuator," in *Robotics and Biomimetics, 2008. ROBIO 2008. IEEE International Conference on*, feb. 2009, pp. 512 –517.

[14] D. N. G. Walker, D.S. Thoma, "Variable impedance magnetorheological clutch actuator and telerobotic implementation," in *Intelligent Robots and Systems, 2009. IROS 2009. IEEE/RSJ International Conference on*, oct. 2009, pp. 2885 –2891.

[15] J. An and D.-S. Kwon, "Haptic experimentation on a hybrid active/-passive force feedback device," in *Robotics and Automation, 2002. Proceedings. ICRA 02. IEEE International Conference on*, vol. 4, 2002, pp. 4217 – 4222 vol.4.

[16] ——, "Stability and performance of haptic interfaces with active/passive actuatorsÃćâĆňâĂĬtheory and experiments," *The International Journal of Robotics Research*, vol. 25, no. 11, pp. 1121–1136, 2006. [Online]. Available: http://ijr.sagepub.com/content/25/11/1121.abstract

[17] O. Baser, E. Konukseven, and H. Gurocak, "Stability and transparency improvement in haptic device employing both mr-brake and active actuator," in *RO-MAN, 2012 IEEE*, sept. 2012, pp. 12 –18.

[18] J. An and D.-S. Kwon, "Virtual friction display of hybrid force feedback interface with actuators comprising dc motor and magnetorheological brake," in *IEEE Industrial Electronics, IECON 2006 - 32nd Annual Conference on*, nov. 2006, pp. 3997 –4002.

[19] Y.-J. Nam and M.-K. Park, "A hybrid haptic device for wide-ranged force reflection and improved transparency," in *Control, Automation and Systems, 2007. ICCAS '07. International Conference on*, oct. 2007, pp. 1015 –1020.

[20] T.-B. Kwon and J.-B. Song, "Force display using a hybrid haptic device composed of motors and brakes," *Mechatronics*, vol. 16, no. 5, pp. 249 – 257, 2006. [Online]. Available: http://www.sciencedirect.com/science/article/pii/S0957415806000122

[21] F. Conti and O. Khatib, "A new actuation approach for haptic interface design," *The International Journal of Robotics Research*, vol. 28, no. 6, pp. 834–848, 2009. [Online]. Available: http://ijr.sagepub.com/content/28/6/834.abstract

[22] C.-M. Chew, G.-S. Hong, and W. Zhou, "Series damper actuator: a novel force/torque control actuator," in *Humanoid Robots, 2004 4th IEEE/RAS International Conference on*, vol. 2, 2004, pp. 533–546 Vol. 2.

[23] P. Fauteux, M. Lauria, M.-A. Legault, B. Heintz, and F. Michaud, "Dual differential rheological actuator for robotic interaction tasks," in *Advanced Intelligent Mechatronics, 2009. AIM 2009. IEEE/ASME International Conference on*, 2009, pp. 47–52.

[24] J. Troccaz, M. Peshkin, and B. Davies, "Guiding systems for computer-assisted surgery: introducing synergistic devices and discussing the different approaches," *Medical Image Analysis*, vol. 2, no. 2, pp. 101 – 119, 1998. [Online]. Available: http://www.sciencedirect.com/science/article/pii/S1361841598800066

[25] F. Periquet and J.Lozada, "A miniature 1-dof mr fluid based haptic interface," *12th International Conference on New Actuators*, pp. 541–544, 2010.

[26] J. Blake and H. Gurocak, "Haptic glove with mr brakes for virtual reality," *Mechatronics, IEEE/ASME Transactions on*, vol. 14, no. 5, pp. 606 –615, oct. 2009.

[27] J. Lozada, M. Hafez, and X. Boutillon, "A novel haptic interface for musical keyboards," in *Advanced intelligent mechatronics, 2007 IEEE/ASME international conference on*, sept. 2007, pp. 1 –6.

[28] B. Liu, W. H. Li, P. B. Kosasih, and X. Z. Zhang, "Development of an mr-brake-based haptic device," *Smart Materials and Structures*, vol. 15, no. 6, p. 1960, 2006. [Online]. Available: http://stacks.iop.org/0964-1726/15/i=6/a=052

[29] L. J. R. S. P. R. A. M. Periquet, F. and M. Hafez, "Mr-drive: A new 1-dof mr fluid based haptic interface," ser. European Mechatronics Meeting (EMM 2009), 2009.

[30] C. Cho, J.-B. Song, and M. Kim, "Energy-based control of a haptic device using brakes," *Systems, Man, and Cybernetics, Part B: Cybernetics, IEEE Transactions on*, vol. 37, no. 2, pp. 341 –349, april 2007.

[31] C. Rossa, J. Lozada, and A. Micaelli, "A new hybrid actuator approach for force-feedback devices," in *Intelligent Robots and Systems (IROS), 2012 IEEE/RSJ International Conference on*, oct. 2012, pp. 4054 –4059.

[32] Q. H. Nguyen and S. B. Choi, "Optimal design of an automotive magnetorheological brake considering geometric dimensions and zero-field friction heat," *Smart Materials and Structures*, vol. 19, no. 11, p. 115024, 2010.

[33] Y.-K. Kong and B. D. Lowe, "Evaluation of handle diameters and orientations in a maximum torque task," *International Journal of Industrial Ergonomics*, vol. 35, no. 12, pp. 1073 – 1084, 2005. [Online]. Available: http://www.sciencedirect.com/science/article/pii/S0169814105000855

[34] Y.-C. Shih and M.-J. J. Wang, "Hand/tool interface effects on human torque capacity," *International Journal of Industrial Ergonomics*, vol. 18, no. 2ÃćâĆňâĂIJ3, pp. 205 – 213, 1996, <ce:title>Towards a New Ergonomics Age in the Pan-Pacific Region</ce:title>. [Online]. Available: http://www.sciencedirect.com/science/article/pii/0169814195000844

[35] C. Rossa, A. Jaegy, J. Lozada, and A. Micaelli, "Design considerations for magnetorheological brakes," *Mechatronics, IEEE/ASME Transactions on*, vol. 19, no. 5, pp. 1669–1680, Oct 2014.

[36] C. Rossa, A. Jaegy, A. Micaelli, and J. Lozada, "Development of a multilayered wide-ranged torque magnetorheological brake," *Smart Materials and Structures*, vol. 23, no. 2, p. 025028, 2014. [Online]. Available: http://stacks.iop.org/0964-1726/23/i=2/a=025028

[37] C. Rossa, J. Lozada, and A. Micaelli, "Stable haptic interaction using passive and active actuators," in *Robotics and Automation (ICRA), 2013 IEEE International Conference on*, 2013.

[38] B. Hannaford and J.-H. Ryu, "Time-domain passivity control of haptic interfaces," *Robotics and Automation, IEEE Transactions on*, vol. 18, no. 1, pp. 1 –10, feb 2002.

[39] R. B. Gillespie and M. R. Cutkosky, "Stable user-specific haptic rendering of the virtual wall," in *Proceedings of the ASME International Mechanical Engineering Congress and Exhibition*, vol. 58, 1996.

[40] D. Senkal and H. Gurocak, "Compact mr-brake with serpentine flux path for haptics applications," in *EuroHaptics conference, 2009 and Symposium on Haptic Interfaces for Virtual Environment and Teleoperator Systems. World Haptics 2009. Third Joint*, March 2009, pp. 91–96.

[41] C. Rossa, L. Eck, A. Micaelli, and J. Lozada, "On a novel torque detection technique for magnetorheological actuators," *Sensors Journal, IEEE*, vol. 14, no. 4, pp. 1223–1231, April 2014.